# Characteristics of relativistic electron mirrors generated by an ultrashort nonadiabatic laser pulse from a nanofilm

Victor V. Kulagin,[1,*] Vladimir A. Cherepenin,[2] Yuri V. Gulyaev,[2] Vladimir N. Kornienko,[2] Ki Hong Pae,[1] Victor V. Valuev,[3] Jongmin Lee,[1] and Hyyong Suk[1,4,†]

[1]*Advanced Photonics Research Institute, GIST, Gwangju 500-712, Republic of Korea*

[2]*Institute of Radioengineering and Electronics, RAS, Mohovaya 11, Moscow 125009, Russia*

[3]*State R&D Laser Center "Raduga," Raduzhnyi, Vladimir Region 600910, Russia*

[4]*School of Photon Science and Technology, GIST, Gwangju 500-712, Republic of Korea*

(Received 3 November 2008; revised manuscript received 1 April 2009; published 13 July 2009)

For controllable generation of an isolated attosecond relativistic electron bunch [relativistic electron mirror (REM)] with nearly solid-state density, we proposed [V. V. Kulagin *et al.*, Phys. Rev. Lett. **99**, 124801 (2007)] to use a solid nanofilm illuminated normally by an ultraintense femtosecond laser pulse having a sharp rising edge (nonadiabatic laser pulse). In this paper, the REM characteristics are investigated in a regular way for a wide range of parameters. With the help of two-dimensional (2D) particle-in-cell (PIC) simulations, it is shown that, in spite of Coulomb forces, all of the electrons in the laser spot can be synchronously accelerated to ultrarelativistic velocities by the first half-cycle of the field, which has large enough amplitude. For the process of the REM generation, we also verify a self-consistent one-dimensional theory, which we developed earlier (cited above) and which takes into account Coulomb forces, radiation of the electrons, and laser amplitude depletion. This theory shows a good agreement with the results of the 2D PIC simulations. Finally, the scaling of the REM dynamical parameters with the field amplitude and the nanofilm thickness is analyzed.

DOI: 10.1103/PhysRevE.80.016404 PACS number(s): 41.75.Jv, 41.75.Ht, 52.38.Kd

## I. INTRODUCTION

Laser generation of attosecond relativistic electron beams is currently a topic of very intense research. Attosecond electron beams can provide time-resolved studies in physics, biology, chemistry, etc., with the attosecond time-scale resolution, which constitutes the main advantage of these beams. Such beams can be used in a large variety of applications, among them are attosecond physics and chemistry [1–3], advanced accelerators and free-electron lasers [4,5], different technological applications, and many other fields. Besides, with the help of ultrashort relativistic electron bunches, bright ultrashort x-ray pulses can be generated using a Thomson backscattering of the probe laser beam [6]. Such pulses are particularly useful for x-ray spectroscopy [7,8] and other applications [9]. If a length and a spread of the electron momenta for an ultrashort electron beam can be small enough, then even coherent x-ray pulses can be generated, which can also be used in many fields [10–12]. In all applications, one needs to control precisely the parameters of the attosecond electron beams, including their length, charge, mean energy, energy spread, and so on.

In high-density (overcritical) plasmas, two mechanisms for generation of ultrashort electron beams—the $\mathbf{v}\times\mathbf{B}$ heating and the vacuum heating—were investigated by two-dimensional (2D) particle-in-cell (PIC) simulations [13,14] and were confirmed by experiments [15,16] recently. Here, Lorentz force ejects electrons one or two times per laser period out of plasma (reflection mode) or accelerates electrons in the low-density preplasma in the direction of the laser pulse with their subsequent penetration through the bulk plasma (transmission mode). Electron ejection and acceleration are irregular in this mechanism, thus explaining the wide energy spread of generated electrons and difficulties with controlling the beam parameters. The length of the electron beam here is about the laser pulse length, besides, the electron beam has a typical microbunching (tapering of density) having laser or half-laser wavelength period (train of electron microbunches). The practical possibility for isolation of a single microbunch is not evident here.

In low-density (underdense) plasmas, ultrashort electron beams can be generated by laser wake field acceleration mechanism [4,17,18]. A single electron bunch can be produced here, but the length of the bunch is usually not shorter than 3–5 $\mu$m (tens of femtoseconds). In a vacuum, a single ultrashort electron beam can be generated through laser compression of a longer electron beam [see, e.g., test particle [19] and one-dimensional (1D) PIC [20,21] simulations]. However, the charge of the bunch here is considerably smaller than 1 pC. The same compression can be applied for thin (1 $\mu$m and less) plasma layers of low (gas) density (1D calculations [22–24]), but the practical realization of such layers is under question now.

We proposed earlier [25] to use a nanofilm (film with a thickness of 10 nm or less) as a solid-state density target for generation of an *attosecond relativistic electron bunch*. It was shown that, when this target is irradiated normally by a superhigh intensity laser pulse with a sharp rising edge (nonadiabatic laser pulse), all electrons of the plasma layer can achieve relativistic longitudinal velocities synchronously when the dimensionless field amplitude becomes large enough, $a_0 \gg \alpha$ [$a_0=|e|E_0/(mc\omega)$, $\alpha=\pi(\omega_p^2/\omega^2)(l/\lambda)$, where

*Present address: Sternberg Astronomical Institute of Moscow State University, Universitetsky prosp. 13, Moscow, Russia. victorvkulagin@yandex.ru

†Corresponding author. hysuk@gist.ac.kr

 

$e$ and $m$ are the charge and the mass of an electron, $c$ is the speed of light, $E_0$, $\omega$, and $\lambda$ are the amplitude, the frequency, and the wavelength of the laser field in a vacuum, $\omega_p = \sqrt{4\pi n_0 e^2/m}$ is the characteristic plasma frequency, and $n_0$ and $l$ are the density and the thickness of the nanofilm]. This scheme has the following features: (i) only a single electron bunch of attosecond length is generated, (ii) the charge of the bunch can be very large (>10 nC), and (iii) the parameters of the bunch can be controlled relatively easily. The diameter of the resulting electron bunch turns out to be considerably greater than its length, so we will call such a bunch a relativistic electron mirror (REM) below. The feasibility for generation of such an attosecond electron bunch was demonstrated for the first time [25] by using virtual experiments, i.e., 2D PIC simulations. It was shown that the new effect of "charge freezing," consisting in a slow (in a time scale of longitudinal acceleration) removal of the electrons from the central part of the REM even when the laser beam diameter is not extremely large, plays an important role in the evolution of the REM and allows for the REM to keep initial surface charge density during all its lifetime. This feature substantially affects the practical realization of the scheme and cannot be derived from the 1D simulations [20,22–24] before. Furthermore, a new self-consistent 1D theory to explain the acceleration process was developed [25]. In the gaslike low-density plasma, consideration of only Coulomb interaction is enough to explain most phenomena [21], but in the solidlike high-density plasma we found that other physics mechanisms such as the laser field depletion, strong radiation of the accelerated electrons, and high radiation friction play very crucial roles in the acceleration process. Hence, our theory includes all of these effects in the model. This theory allows us to calculate all parameters of the REM electrons, i.e., trajectories, momenta, energies, etc., and turns out to be in a good agreement with the 2D PIC simulations.

In this paper, the REM characteristics are investigated in a regular way for a wide range of parameters. With the help of the 2D PIC simulations, we study the role of the laser pulse amplitude and the nanofilm parameters (thicknesses and density) in the process of REM generation. For different nanofilm density and constant thickness, we (i) determine the laser amplitude threshold for the process of the REM generation, (ii) reveal the dependences of the maximal energy of electrons, the energy spread, and the lifetime of the REM on the field amplitude and parameter $\alpha$, and (iii) compare the PIC results with the predictions of the self-consistent 1D theory [25] and verify a good agreement. Besides, we investigate the dependence of the REM parameters on initial thickness of the nanofilm with constant parameter $\alpha$ (initial density was changed in accordance with initial thickness). And finally based on the developed theory, the scaling of the REM dynamical parameters with the field amplitude and the nanofilm thickness is analyzed.

The main condition for realization of the proposed generation scheme is the availability of nonadiabatic laser pulses. Recently, a few-cycle laser pulses with very sharp fronts have been generated experimentally [26,27] and, in the near future, one can expect the generation of few-cycle laser pulses of petawatt and even exawatt ($10^{18}$ W) levels [28]. The other problem for experimental realization of the proposed scheme is the production of a nanofoil. Solid films with a thickness of around 10 nm are available routinely in experiment [29–31]. However, as we will show below, the better results in terms of maximal energy and energy spread can be achieved for the smaller thickness of the target around 1–3 nm. In this case, graphene sheets [32–34] can be used as a target. The other possibility is to use liquid crystal films, which thickness can be adjusted by changing the temperature [35–37].

If attosecond electron bunches are expected to be used for injection or other stand-alone applications, they can be extracted from the electromagnetic wave just at their peak energy with the help of a plasma separator [38–40]. For generation of an attosecond high-frequency electromagnetic radiation with the help of the REM, extraction of the attosecond electron beams from an electromagnetic wave is not necessary. In this case, the REM can be directly used for Thomson backscattering a probe counterstreaming laser pulse with frequency upshifting and amplitude enhancement. One-dimensional studies of this process are presented in [22–24,41], where the requirements for the REM parameters and characteristics of the up-shifted probe beams are specified. This two-pulse method allows us, in principle, to control all parameters of the converted electromagnetic pulse in a full extent (duration, frequency, shape of an envelope, carrier-envelope phase, etc.) in contrast with the case of a one-pulse method of overcritical plasma excitation [42] or with the case of free-electron lasers [43], where it is not easy to change the parameters of the produced pulse. In the two-pulse generation scheme, dynamical properties of the REM directly influence the statistics of the generated high-frequency radiation. Therefore, an investigation of the dynamic behavior and parameters of the REM is a very important issue. Some recent studies on these problems can be found in [44,45].

The paper is organized as follows: PIC simulations for the REM generation are presented in Sec. II. In Sec. III, one-dimensional theory for the REM generation is derived. In Sec. IV, REM characteristics for different parameters are specified and comparison between the 1D theory and the 2D PIC simulations is presented. In Sec. V, the change in the REM parameters with nanofilm initial thickness (keeping $\alpha$ constant) is analyzed. The scaling of the REM parameters with $\alpha$ and laser pulse amplitude $a_0$ is considered in Sec. VI. Section VII concludes the discussion.

## II. PIC SIMULATIONS FOR THE REM GENERATION

To study the characteristics of the REM, we performed 2D PIC simulations with the OSIRIS [46] and with the XOOPIC [47] codes. We used linearly $y$-polarized laser pulses ($\lambda = 1$ $\mu$m), running along the $z$ axis in the positive direction and having two different beam waists $w_0$ at focus: $kw_0=50$ (laser spot size is $2w_0 \approx 16\lambda$) and $kw_0=12.5$ (laser spot size is about $4\lambda$), where $k=2\pi/\lambda$. To reduce the Coulomb expansion of the REM, one needs to decrease $\alpha$, which is proportional to the surface density of electrons $n_0 l$ [22–24,48]. So in simulations, we used three different nanofilms (positioned at the beam focus) with the parameter $\alpha$ equals 1, 3, or 10.

These correspond to the nanofilms with thickness from 1 to 10 nm if a reasonable solid-state density $n_0=318.3n_{cr}$ is considered, where $n_{cr}$ is the critical density (for convenience, in the PIC simulations, we changed the density instead of the thickness). The plasma was assumed to be preionized and collisionless with the ions mass $m_i=3671m$. A laser pulse with a Gaussian transverse profile and a steplike longitudinal envelope was used; the duration of the laser pulse was 3λ. The physics of the REM generation depends primarily on the ratio $a_0/\alpha$ [25]. So to reduce the simulation time and to achieve a reasonable accuracy, the set of laser pulse amplitudes for each $\alpha$ was chosen as $a_0=4\alpha$, $a_0=6\alpha$, and $a_0=10\alpha$. In the simulations, the so-called moving window technique was adopted. For the OSIRIS simulations, we used 630 grid points per λ along the longitudinal direction and $16(w_0\approx 8\lambda)$ or $63(w_0\approx 2\lambda)$ grid points per λ along the transverse direction, and 256 particles per cell were employed (total number of particles is about $8\times 10^5$). Generally speaking, XOOPIC simulations require several times more grid points per λ to achieve the accuracy similar to that of the OSIRIS simulations, however, each time step is calculated faster with the XOOPIC code. So, for the laser pulse amplitudes of $4\alpha$ and $6\alpha$, we used 2500 grid points per λ along the longitudinal direction and 20 grid points per λ along the transverse direction (for the XOOPIC simulations, only the laser pulse with $w_0\approx 8\lambda$ was used), and 200 particles per cell were employed (total number of particles is about $4\times 10^6$). For the longer XOOPIC simulations with $a_0=10\alpha$, we used 10 000 grid points per λ along the longitudinal direction with 50 particles per cell (but still the accuracy of the simulations was lower than for the two previous cases).

Phase spaces $z-y$ and $p_z-y$ (the momentum $p_z$ is normalized by $mc$) are presented for two different times, $t=2.1T_0$ and $t=3.2T_0$, in Fig. 1 (see also [25]). Here $w_0\approx 8\lambda$, $T_0$ is the laser cycle, the direction of the laser pulse is shown with the red arrow, and the motion of the electrons is recalculated into the laboratory system. These phase spaces (and all other simulation results in this section) were obtained with the OSIRIS code for $\alpha=10$ and $a_0=60$. The electrons near the laser beam axis ($y=16\lambda$) form the REM. Due to a snowplow action of the laser pulse [22–24,49], all electrons are removed from the central part of the nanofilm and are accelerated longitudinally to relativistic velocities. Because of large Coulomb forces, the electrons in the left side of the REM (called left electrons below) turn back at some time while other electrons continue to move to the right. Thus, left electrons on the laser beam axis turn back at about $t\simeq 3.82T_0$ (cf. Fig. 3); this time can be defined as a lifetime $t_l$ of the REM for $\alpha=10$ and $a_0=60$. The position of the first turning point of the left electrons depends primarily on the ratio of the parameters $a_0$ and $\alpha$. Therefore, because of the Gaussian transverse profile of the laser pulse, the diameter of the REM gradually decreases with time (for $t\simeq t_l$, the diameter of the REM is about zero). However, even after the turn of all left electrons, major part of the electrons continues to move, forming partial REM with the full thickness of about λ. On the edges of the REM, the laser pulse produces usual heating of the plasma (e.g., near $y=8\lambda$ and $y=24\lambda$ in Fig. 1).

During acceleration, the REM "eats away" the first half-cycle of the laser pulse (amplitude transmission is less than

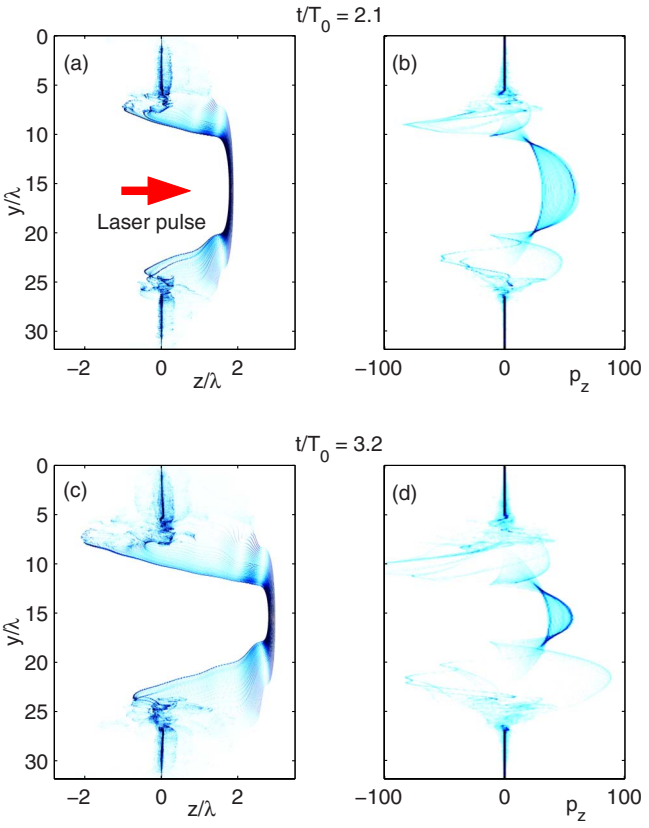


FIG. 1. (Color online) Phase spaces (a) and (c) $z-y$ and (b) and (d) $p_z-y$ for the electrons accelerated by the laser pulse having the waist $w_0\approx 8\lambda$ [25] for $t=2.1T_0$ (upper panels) and $t=3.2T_0$ (lower panels), where $T_0$ is the laser cycle. The direction of the laser pulse is shown with the red arrow.

10%), so by the end of the REM lifetime, the first half-cycle of the laser pulse almost totally disappears. On the other hand, the subsequent laser half-cycles remain almost intact so the parameters of the REM depend mainly on the first half-cycle, which generates the REM.

The phase spaces for $w_0\approx 2\lambda$ and $\alpha=10$, $a_0=60$ (Fig. 2) look very similar to those presented in Fig. 1, with the only important differences being the fourfold decrease in the REM dimension along the $y$ axis and larger asymmetry of the plots, which arises due to the more evident motion of the REM electrons in laser field along $y$ direction. The lifetime for this case is about $t_l\simeq 3.7T_0$. This means that the considered process is effectively quasi-one-dimensional and has a regular character.

We suppose below that just the most left and the most right electrons define the REM longitudinally. Actually, a more rigorous definition can involve the notion of the critical density $n_{cr}$, i.e., the edges of the REM can be defined as points, where the density of the REM is equal to $n_{cr}$. In this case, to get the smooth electron density dependence, one needs to average the cell density over several grid cells. All the grid cells on the laser beam axis below the most left electrons and above the most right electrons are empty (cf. the insets of Fig. 3). So with the averaging procedure, the rigorously defined boundaries of the REM will be several grid cells away from the boundaries, defined with our ap-

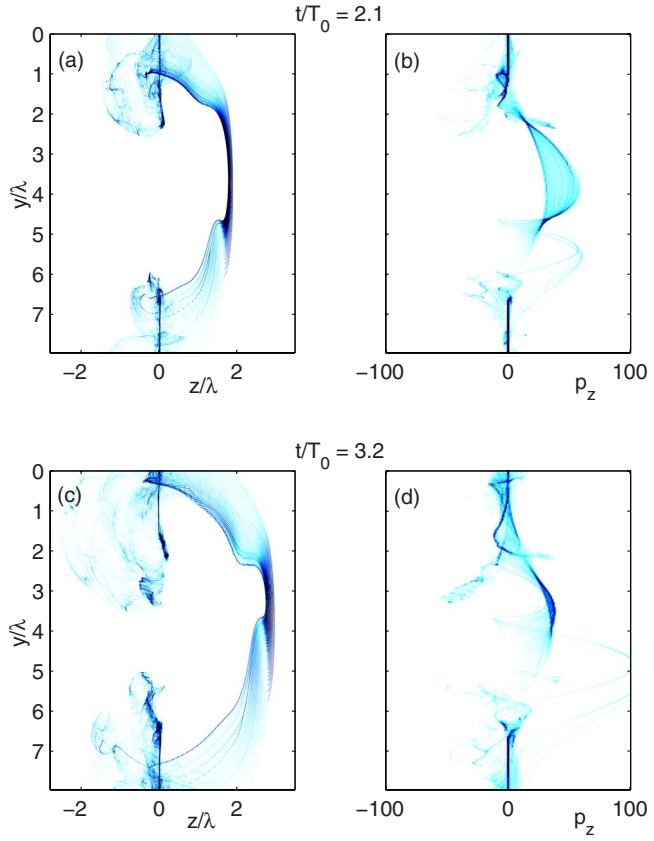


FIG. 2. (Color online) Phase spaces (a) and (c) $z-y$ and (b) and (d) $p_z-y$ for the electrons accelerated by the laser pulse having the waist $w_0 \approx 2\lambda$ for $t=2.1T_0$ (upper panels) and $t=3.2T_0$ (lower panels). Note the different vertical scales here and in Fig. 1

proach. For the fine grids in our simulations, the difference between two definitions occurs to be negligible, but our definition is much simpler that is why we adopted it. Besides, as we will see in Sec. V, for such a thin target, the physics of

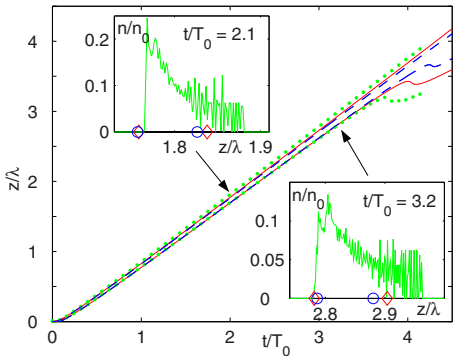


FIG. 3. (Color online) Coordinates of the most left and the most right electrons of the REM as functions of time [25]: green dots are the results for the 2D PIC simulations with $\alpha=10$, $a_0=60$, and $w_0 \approx 8\lambda$ taken on the laser beam axis ($y=16\lambda$), red solid lines and diamonds are the numerical solutions of systems (7), and blue dashed lines and circles are the approximate analytical solutions according to Eqs. (10). In insets, the electron densities (normalized by the initial density $n_0$) on the laser beam axis for $t=2.1T_0$ and $t=3.2T_0$ are presented (green solid lines).

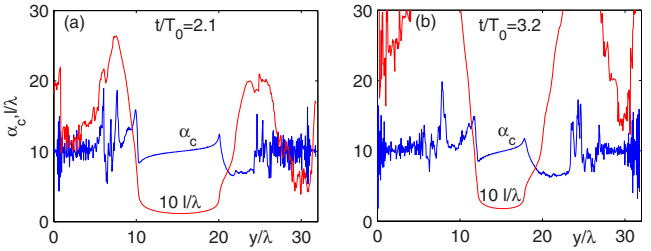


FIG. 4. (Color online) Thickness $l$ (multiplied by 10, red line marked with symbols $10l/\lambda$) and surface charge density $\alpha_c$ (blue line marked with symbol $\alpha_c$) for the REM with $\alpha=10$ [25] formed by the laser pulse with the amplitude $a_0=60$ and the waist $w_0 \approx 8\lambda$ [(a) $t=2.1T_0$ and (b) $t=3.2T_0$]. The REM itself stretches approximately from $y=10\lambda$ to $y=20\lambda$ on plot (a) and from $y=12\lambda$ to $y=17\lambda$ on plot (b).

interaction is determined primarily by the parameter $\alpha$ (and $a_0$) and not by the density of the target only (in contrast with a case of a semi-infinite plasma).

The coordinates of the most left and the most right electrons of the REM as functions of time for the case of $\alpha=10$, $a_0=60$, and $w_0 \approx 8\lambda$ are shown in Fig. 3 [25]. The full thickness of the REM in the central part is considerably smaller than $\lambda$ (see also Fig. 4) right up to the first turning point of the left electrons, where it is about $\lambda/2(kl \simeq \pi)$. The full thickness of the REM near $t=2.1T_0$ (where the momenta $p_z$ of the REM electrons are close to the maxima; cf. Sec. IV) is only about $\lambda/10$ (cf. insets of Fig. 3), i.e., about 300 as (the full length at half maximum here is only about 90 as). Such a small thickness is provided partially by the very small initial value for $l$ and partially by the compressing magnetic forces due to synchronous movement of the electrons along the $y$ direction [22,24]. Also, the REM remains strongly overcritical during all the lifetime.

The full thickness $l$ (multiplied by 10) and the surface charge density $\alpha_c$ of the REM as functions of the transverse coordinate $y$ are presented in Fig. 4 ($\alpha=10$, $a_0=60$, and $w_0 \approx 8\lambda$) for two different times (see also [25]). It is remarkable that, during the evolution, the surface charge density $\alpha_c$ of the REM remains close to the initial value $\alpha=10$ for the nanofilm, and there is almost no charge removal from the central part of the REM to the peripheral parts even for a moderate diameter of the laser beam. We called this feature a charge freezing effect of the superintense nonadiabatic laser pulse as opposed to the well-known drilling effect of an adiabatic laser pulse. Also, inside the REM, $l$ and $\alpha_c$ change smoothly indicating the coherence of the electron movements contrary to the outer regions, where the electrons move chaotically and $\alpha_c$ changes very rapidly. The same figures for the smaller beam size $w_0 \approx 2\lambda$ are presented in Fig. 5, where the background electrons near the initial position of the nanofilm were removed during calculation (cf. Fig. 2). Again, the graphics in this figure are very similar to Fig. 4 with rescaling of the $y$ axis by four times, and the greater asymmetry can be seen.

So the REM is a transient coherent structure, in which all electrons move synchronously. It exists only for a limited period of time. In the above simulations, the lifetime of the REM is about four laser periods (13 fs). Larger values for $a_0$

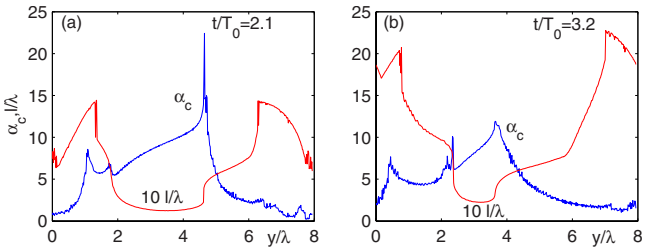


FIG. 5. (Color online) Thickness $l$ (multiplied by 10, red line marked with symbols $10l/\lambda$) and surface charge density $\alpha_c$ (blue line marked with symbol $\alpha_c$) for the REM with $\alpha=10$ formed by the laser pulse with the amplitude $a_0=60$ and the waist $w_0\approx 2\lambda$ [(a) $t=2.1T_0$ and (b) $t=3.2T_0$; background electrons are removed]. Note the different horizontal scales here and in Fig. 4

or smaller values for $\alpha$ can increase the lifetime of the REM up to tens (see below) or even hundreds of femtoseconds [24]. If $a_0$ is less than some threshold, which depends on $\alpha$, the REM will not be formed at all (cf. Sec. IV), and only the well-known heating of the plasma by the laser pulse [13,15,16] will result.

## III. ONE-DIMENSIONAL THEORY FOR THE REM GENERATION

Let us now elaborate the 1D theory for the generation of the REM [25]. The nanofilm will be modeled with a set of electron sheets (ESs), each numbered by its initial coordinate $z_0\in[0,l]$. The laser field will be modified by virtue of an interference with radiation emitted by these ESs, and the motion of the ESs will be defined by the combined electromagnetic field (the self-consistent model should be used here since $\alpha\geq 1$ and the modification of the initial laser field is considerable [22,24]). The fields of one ES can be determined by 1D analogs of the classical Lienard-Wiechert solutions [22,24,50],

$$E_z(z,t)=2\pi\sigma\,\mathrm{sgn}[z-Z(t')],$$

$$\mathbf{E}_{\perp e}(z,t)=-2\pi\sigma\frac{\boldsymbol{\beta}_\perp(t')}{1-\beta_z(t')\mathrm{sgn}[z-Z(t')]},$$

$$\mathbf{H}_e(z,t)=\frac{2\pi\sigma\,\mathrm{sgn}[z-Z(t')][\boldsymbol{\beta}_\perp(t')\times\mathbf{e}_z]}{1-\beta_z(t')\mathrm{sgn}[z-Z(t')]},\qquad(1)$$

where $\mathbf{E}_{\perp e}=E_{xe}\mathbf{e}_x+E_{ye}\mathbf{e}_y$, $\mathbf{v}_\perp=v_x\mathbf{e}_x+v_y\mathbf{e}_y$, and $t'$ is the retarded time,

$$c(t-t')=|z-Z(t')|.\qquad(2)$$

In these equations, we suppose that charge and current densities for the ES are $\rho(z,t)=\sigma\delta[z-Z(t)]$ and $\mathbf{j}(z,t)=\sigma\mathbf{v}(t)\delta[z-Z(t)]$, where $\sigma$ is the surface charge density for the ES and $Z(t)$ is the longitudinal coordinate of the ES.

The total field of the plasma layer is equal to the sum of the fields of all ESs,

$$E_{zs}(z,t)=2\pi en_0\int_0^l\mathrm{sgn}[z-Z(z_0,t)]dz_0,$$

$$\mathbf{E}_{\perp s}(z,t)=-2\pi en_0\times\int_0^l\frac{\boldsymbol{\beta}_\perp[z_0,t'(z,z_0,t)]}{1-\mathrm{sgn}[z-Z(z_0,t)]\cdot\beta_z[z_0,t'(z,z_0,t)]}dz_0,$$

$$\mathbf{H}_s(z,t)=2\pi en_0\times\int_0^l\frac{\mathrm{sgn}[z-Z(z_0,t)]}{1-\mathrm{sgn}[z-Z(z_0,t)]\cdot\beta_z[z_0,t'(z,z_0,t)]}\times\boldsymbol{\beta}_\perp[z_0,t'(z,z_0,t)]\mathbf{e}_z dz_0,\qquad(3)$$

where $Z(z_0,t)$ is the longitudinal coordinate of the ES with the initial coordinate $z_0\in[0,l]$ and the retarded time $t'(z,z_0,t)$ is different for different ESs and can be determined by Eq. (2).

Inserting these expressions into equations of motion for the ES with the coordinate $z_0$, one can arrive at the nonlinear integrodifferential equation with delay [24], which contains the ES variables only. In general case, this equation can be solved only numerically; the solution should be computed for a large number of ESs simultaneously to evaluate the integrals that requires large computational resources.

To reduce the system, we will use the following simplifying assumptions. Our goal is to describe the initial coherent stage of the nanofilm's evolution when the thickness of the nanofilm is small, $l\ll\lambda$, and there is neither heating of the nanofilm nor turbulent motion of the ESs. Then, we assume that (i) the radiation field of each ES immediately acts on the other ESs (so there is no delay and $t'\simeq t$) and (ii) there are no intersections of trajectories of the ESs [so the Coulomb force between each ES and other ESs are constant in time; cf. first equation in Eqs. (3)]. Besides, the field amplitude is supposed to be high and $l\ll\lambda$, so we assume that (iii) the ESs are immediately removed from the ion layer after beginning of the interaction (so the Coulomb force acting on each ES from the ions is also constant in time). Then, we obtain for the ES with the initial coordinate $z_0$ the following equations of motion:

$$\frac{dp_y}{d(\omega t)}=-a_0e_y\frac{\kappa}{\gamma}-\alpha\left[I_1\frac{\kappa}{\gamma}+I_2\frac{1+p_y^2}{\kappa\gamma}\right],$$

$$\frac{d\kappa}{d(\omega t)}=\frac{2\alpha}{\gamma}\left[\kappa\left(\eta-\frac{z_0}{l}\right)-p_yI_2\right],\qquad(4)$$

where $e_y=\sin(\omega t-kz)$ is the time dependence of the laser field, $\boldsymbol{p}=\gamma\mathbf{v}/c$ is the normalized momentum of the electrons with velocity $\mathbf{v}$, $\gamma=(\sqrt{1-v^2/c^2})^{-1}$, and $\eta=\eta[Z(z_0,t)]$ is the step function: $\eta(x)=0$ for $x<0$ and $\eta(x)=1$ for $x>0$. The integrals $I_1(z_0,t)$ and $I_2(z_0,t)$ are defined by the following expressions:

$$I_1(z_0,t)=l^{-1}\int_0^{z_0}\frac{p_y(z_0',t)dz_0'}{\kappa(z_0',t)},$$

$$I_2(z_0,t) = l^{-1}\int_{z_0}^{l} \frac{p_y(z_0',t)\kappa(z_0',t)dz_0'}{1+p_y^2(z_0',t)}. \tag{5}$$

Physically, the integral $I_1$ describes the action of the radiation field of all left ESs on the ES with coordinate $z_0$ and $I_2$ describes the action of the radiation field of right ESs. Thus, the integrals $I_1$ and $I_2$ provide for collective radiation friction force, which acts on the ES with coordinate $z_0$, and the model is fully electromagnetic (note that a "true" radiation friction force, which originates from the own radiation of this ES, can be neglected when the total number of the ESs is large enough and their motion is coherent).

Above, we introduce the parameter $\kappa=\gamma-p_z$. Then as usual, $\gamma$ and $p_z$ can be calculated with equations

$$\gamma = \frac{1+p_y^2+\kappa^2}{2\kappa},$$

$$p_z = \frac{1+p_y^2-\kappa^2}{2\kappa}. \tag{6}$$

Equations (4) are derived for the coherent evolution of the nanofilm when $l$ stays considerably smaller than $\lambda$; so to evaluate the integrals $I_1$ and $I_2$, we suppose that the integrands in Eqs. (5) can be represented in any internal point $z_0 \in [0,l]$ as a linear interpolation of their values on the ends of the interval, i.e., at points $z_0=0$ and $z_0=l$. Then, one has that $\kappa_l=1$ and

$$\frac{dp_{y0}}{d(\omega t)} = -a_0 e_y\frac{\kappa_0}{\gamma_0} - \frac{\alpha}{2\gamma_0}\left(p_{y0} + \frac{p_{yl}}{\kappa_0}\frac{1+p_{y0}^2}{1+p_{yl}^2}\right),$$

$$\frac{d\kappa_0}{d(\omega t)} = \frac{\alpha\kappa_0}{\gamma_0}\left[2\eta(Z_0) - \frac{p_{y0}^2}{1+p_{y0}^2} - \frac{p_{y0}p_{yl}}{\kappa_0(1+p_{yl}^2)}\right],$$

$$\frac{d(kZ_0)}{d(\omega t)} = \frac{1+p_{y0}^2-\kappa_0^2}{1+p_{y0}^2+\kappa_0^2},$$

$$\frac{dp_{yl}}{d(\omega t)} = -\frac{a_0 e_y}{\gamma_l} - \frac{\alpha}{2\gamma_l}\left(p_{yl} + \frac{p_{y0}}{\kappa_0}\right), \tag{7}$$

where indices 0 and $l$ stand for the left ($z_0=0$) and the right ($z_0=l$) ESs. So equations of motion of all ESs are reduced now to the coupled nonlinear system of equations for the two outer ESs, which can be easily solved numerically.

A further step is to derive some analytical insight into the dynamical characteristics of the nanofilm. As one can see, Eqs. (7) have no exact analytical solutions. To uncouple equations for the left and the right ESs and to get the approximate analytical solutions, we suppose that $p_{y0}/\kappa_0 = p_{yl}/\kappa_l = p_{yl}$ in the large brackets of the right-hand sides of Eqs. (7) (i.e., in terms originating from the self-action of the collective radiation of the nanofilm). Actually, the ratio $p_y/\kappa$ of some ES is proportional to the right-going radiation of this ES, for the initial coherent stage of evolution, this radiation depends mainly on the external field of the laser pulse, and for $l \ll \lambda$, this external field is the same for the left and the right ESs. After decoupling, we transfer to new independent variables $\theta_0=\omega t-kZ_0$ and $\theta_l=\omega t-kZ_l$, where $Z_0$ and $Z_l$ are the $z$ coordinates of the right and the left ESs (we consider $Z_0>0$ only),

$$\frac{dp_{y0}}{d\theta_0} = -a_0 e_y - \alpha\frac{p_{y0}}{\kappa_0}\left(1+\frac{\kappa_0^2}{2(\kappa_0^2+p_{y0}^2)}\right),$$

$$\frac{d\kappa_0}{d\theta_0} = \alpha\left[\frac{1}{1+p_{y0}^2} + \frac{\kappa_0^2}{\kappa_0^2+p_{y0}^2}\right],$$

$$\frac{dp_{yl}}{d\theta_l} = -a_0 e_y - \alpha p_{yl}. \tag{8}$$

Then, equation for the right ES can be solved exactly. Two equations describing the motion of the left ES still have to be modified. The parameter $\kappa_0$ is a slow function since its derivative depends on $p_{y0}^{-2}$ and, hence, on $a_0^{-2}$. Then, equation for $p_{y0}$ can be approximately solved using the slowness of $\kappa_0$ and supposing that $\kappa_0 \ll |p_{y0}|$ [cf. the second equation in systems (10)]. Substituting simplified solution $p_{y0} = a_0\kappa_0\alpha^{-1}\sin\theta_0$ into the equation for $\kappa_0$ in Eqs. (8) and integrating this equation by $\theta_0$ over the period of the laser field to remove the fast $\theta_0$ dependence, one can get the following equation for $\kappa_0$, in which only the slow evolution with $\theta_0$ is retained:

$$\frac{d\kappa_0}{d\theta_0} = \alpha^2\left[\frac{1}{\sqrt{\alpha^2+a_0^2\kappa_0^2}} + \frac{1}{\sqrt{\alpha^2+a_0^2}}\right]. \tag{9}$$

For the case of large $a_0$ with respect to $\alpha$, one can get an implicit equation for $\kappa_0$ after integration. Solving this implicit equation approximately, we obtain eventually the following parametric solutions for Eqs. (8) with parameters $\theta_0$ and $\theta_l$:

$$\kappa_0 = 1 + \frac{\alpha^2\theta_0}{a_0} + \ln\left(1+\frac{\alpha^2\theta_0}{a_0}\right),$$

$$p_{y0} = -\frac{a_0\kappa_0}{\kappa_0^2+\alpha^2}\left\{\alpha\sin\theta_0 - \kappa_0\left[\cos\theta_0 - \exp\left(-\frac{\alpha\theta_0}{\kappa_0}\right)\right]\right\},$$

$$kZ_0 = \int_0^{\theta_0}\frac{(1+p_{y0}^2)d\theta_0'}{2\kappa_0^2} - \frac{\theta_0}{2},$$

$$p_{yl} = -\frac{a_0}{1+\alpha^2}[\alpha\sin\theta_l - \cos\theta_l + \exp(-\alpha\theta_l)],$$

$$kZ_l = \int_0^{\theta_l}\frac{p_{yl}^2 d\theta_l'}{2},$$

$$\omega t = \theta_0 + kZ_0 = \theta_l + kZ_l. \tag{10}$$

In Fig. 3, the solutions for Eqs. (7) are shown with red solid lines and diamonds and the solutions for Eqs. (10) are shown with blue dashed lines and circles. From Fig. 3, one can conclude that these solutions coincide well with the PIC re-

sults almost until the first turning point of the left ES at $t \simeq 3.82T_0$. The small difference can be explained as follows. Omitting the retardation for the radiation fields of the ESs increases the synchronism in the motion of the ESs that results in smaller thickness of the REM and longer period of coherent evolution (longer time until first turn of the left electrons of the REM). These features can be found in Fig. 3. However, from the insets of Fig. 3, one can see that the analytical approach describes well the main peak of the electron density discarding only the low-density part of the REM. So the elaborated analytical approach [reduced systems (7) and the approximate solutions of systems (10)] can be used for quick calculation of the dynamical parameters of the REM. Comparison of the theory with the 2D PIC simulations for the wide range of parameters is presented in Sec. IV.

## IV. REM CHARACTERISTICS FOR DIFFERENT $\alpha$ AND $a_0$ AND COMPARISON WITH THE THEORY

Let us now examine the characteristics of the REMs generated from the nanofilms with $\alpha$ equals 1, 3, or 10 by the laser pulse with the amplitudes $a_0=4\alpha$, $a_0=6\alpha$, and $a_0=10\alpha$. In this section, the XOOPIC code will be used for simulations.

The first question relevant for the production of the REM by the laser pulse is the question about a threshold of generation, i.e., the laser pulse of what amplitude can generate the REM for some fixed value of $\alpha$ (or the nanofilm thickness). In principle, there is no strict definition for the threshold. Actually, a laser pulse of any amplitude produces some longitudinal displacement of the electrons. However, having in mind the application of the REM as a reflector for a probe laser beam, it is reasonable to consider that the laser pulse has threshold amplitude if the duration of the forward longitudinal motion of the left electrons from their initial positions (or, equivalently, the lifetime of the REM) is equal to the laser period $T_0$. (That is, the total time of displacement in the forward direction is about $2T_0$. Note that for a small amplitude of the laser pulse, an electron executes a "figure-of-eight" motion in the laser field [51] so the duration of the forward motion is about $T_0/4$.) With this criterion, the threshold values of the laser pulse amplitude are shown in Fig. 6. These values were obtained using the 2D PIC simulations, and the simulated points are marked with squares. For calculations of the thresholds (and for all other calculations within this section), the electrons near the laser beam axis were considered. It is interesting to note that all simulated points belong practically to the same straight line, which crosses the axis $\alpha=0$ at $a_0 \approx 1$. Then, from the simulation data, one can derive the following phenomenological formula for the threshold amplitude of the REM generation:

$$a_{0th} = 0.92 + 2.61\alpha. \tag{11}$$

So to generate the REM, one need the laser pulse amplitude, which is approximately tree times larger than the parameter $\alpha$. Therefore, it is difficult to generate the REM from the thick film, and for modern laser systems, the maximal thickness of the nanofilm should be not greater than 20 nm (which requires $a_0 \simeq 60$).

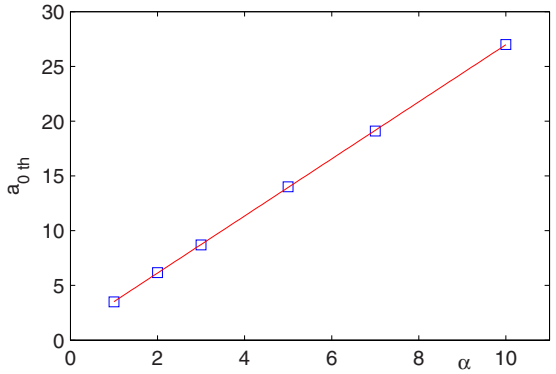


FIG. 6. (Color online) Threshold amplitudes of the laser pulse required for generation of the REM. The simulated points are marked with blue squares; the red line is a best linear fit to the simulated points.

For applications, several dynamical parameters of the REM can be of great importance. These are lifetime of the REM, maximal energy and energy spread of the REM electrons, thickness of the REM (or, equivalently, the length of the REM), etc. As was shown in Sec. II, the left electrons of the REM turn back at $t_l$ (and obviously, their energy has maximum on $t_l$), while the right electrons can continue the forward motion for a long time (and their energy can be monotonous on $t_l$). We are interested in the evolution of the REM within the lifetime $t_l$, so it is reasonable to characterize the REM by considering the evolution of the left electrons. The energy and transverse and longitudinal momenta of some ES as functions of time are shown in Fig. 7. These plots were obtained with the help of a self-consistent 1D code EXACT [50], in which the system of equations for the ES motion, utilizing Eqs. (3) for the total field of the ESs, was solved numerically. In Fig. 7, the meanings of the dynamical parameters of the REM, which are analyzed below, are also clarified. So below, we calculate the REM lifetime $t_l$ as the time at which the longitudinal momentum of the left REM electrons near the laser beam axis becomes equal to zero. The maximal energy $\gamma_{\max}$ of the REM electrons is considered as the maximal energy of the left electrons within the lifetime $t_l$. If this happens at time $t_{\gamma\max}$, then the minimal energy of the REM electrons is the energy of the right electrons at time $t_{\gamma\max}$. The energy spread is calculated as half of the difference between the energies of the left and of the right electrons at this time: $\Delta\gamma=0.5|\gamma_{\max}-\gamma_{\min}|$.

The 2D PIC simulation results for a set of parameters are presented in Fig. 8 by green stars (here and below, all lines between simulation points were added only for better readability of the plots). In the left column, the results for the REM with $\alpha=1$ are shown, in the second column, $\alpha=3$, and in the third column, $\alpha=10$. The first row of the plots shows the maximal $\gamma_{\max}$ and the minimal $\gamma_{\min}$ energies of the REM electrons, second row presents the lifetime $t_l$ and the time $t_{\gamma\max}$, at which the energy of left electrons reaches maximum, and the third row shows the length $l_\gamma$ of the REM at time $t_{\gamma\max}$ (from Fig. 3, one can conclude that the length increases monotonously during the lifetime).

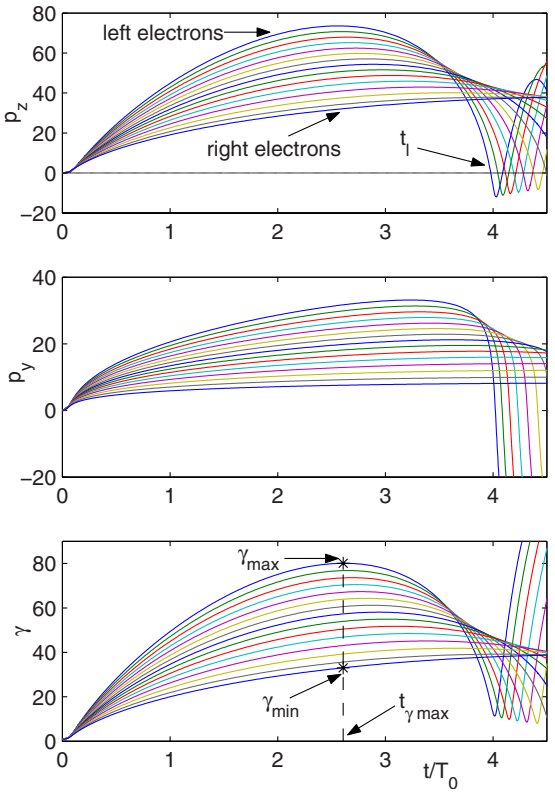


FIG. 7. (Color online) Longitudinal momenta, transverse momenta, and energies of some ESs of the REM as functions of time for $a_0=60$ and $\alpha=10$. The meanings of the dynamical parameters of the REM, which are analyzed below, are clarified.

In Fig. 8, the theoretical values for the same parameters are also presented. The values, calculated from the numerical solution of the system of Eqs. (7), are shown with red diamonds and the values from approximate analytical solutions (10) are shown with blue circles. Here, one can observe the same feature as in Fig. 3: the values calculated with the numerical solution of systems (7) are closer, in general, to the PIC values than those estimated from analytical solutions (10). On the other hand, all these three sets of values turn out to be close enough in a wide range of the REM parameters showing the adequacy of the theory.

One can make several conclusions based on the results presented in Fig. 8. First of all, absolute value for the energy spread of the REM electrons decreases with decrease in $\alpha$, and for small values of $\alpha$, the energy spread can be very small, i.e., the REM can be quasimonochromatic in energy. This is very important for applications. Also, from the first row of Fig. 8, one can conclude that, for large values of $\alpha$, the energy grows almost linearly with $a_0$, contrary to the case of small values of $\alpha$, where the energy growth is practically quadratic [cf. also a case of a low-density electron beam in a superintense laser field [20], where the energy grows quadratically, and Eqs. (15) and (16) below]. This feature constitutes the role of the collective radiation friction force for the electrons of the nanofilm [50].

Next, the lifetime of the REM grows quadratically with $a_0$ [see also Sec. VI and Eq. (18)] and, for the large values of $\alpha$, depends primarily on the ratio $a_0$ to $\alpha$ (cf. the corresponding curves for $\alpha=3$ and $\alpha=10$). Thus, for $a_0/\alpha=10$, the lifetime is around $10T_0$ or 33 fs that is enough for many applications. It is interesting to note also that the ratio of $t_{\gamma\,max}$ to $t_l$ is close to the value of 0.6 for any combination of the considered parameters, the deviation of the ratio from this value being less than 10%.

And at last, the length $l_\gamma$ of the REM at time $t_{\gamma\,max}$ decreases with $a_0$ and increases with $\alpha$. However, for all considered cases, the length $l_\gamma$ of the REM remains near the level $\lambda/10$ or less assuming good opportunities for use.

The relative value for the energy spread of the REM electrons calculated from the 2D PIC simulations is presented in Fig. 9. The relative energy spread is calculated as $\Delta\gamma/\gamma_{av}$, where the average value for the energy of the REM electrons

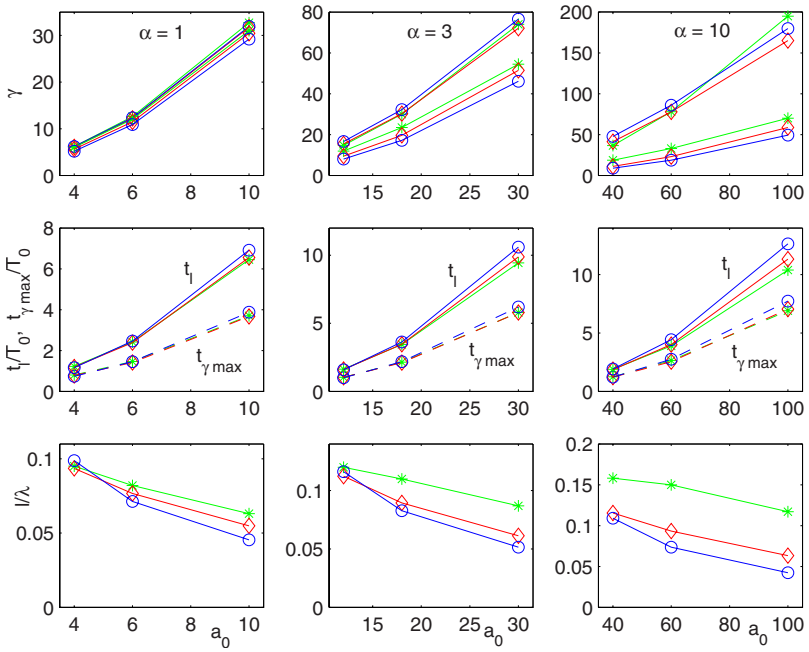


FIG. 8. (Color online) Dynamical parameters of the REM as functions of $a_0$ for different values of $\alpha$. The maximal $\gamma_{max}$ and the minimal $\gamma_{min}$ energies of the REM electrons are shown in the first row of the plots. The lifetime $t_l$ of the REM and the time $t_{\gamma\,max}$, when the energy of the left REM electrons reaches maximum, are presented in the second row of the plots (solid lines and dashed lines, correspondingly). The length $l_\gamma$ of the REM at time $t_{\gamma\,max}$ is shown in the third row of the plots. The first column is for $\alpha=1$, the second is for $\alpha=3$, and the third is for $\alpha=10$. The PIC results are presented by green stars, the numerical results from Eqs. (7) are shown with red diamonds, and the approximate analytical solutions from Eqs. (10) are shown with blue circles (lines connecting the simulation points were added only for better readability of the plots).

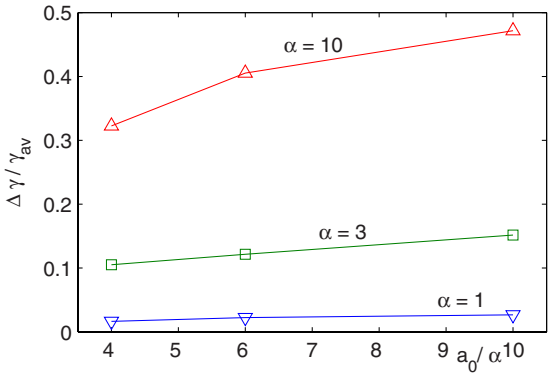


FIG. 9. (Color online) Relative value for the energy spread of the REM electrons for different values of $\alpha$ as functions of $a_0$. The case of $\alpha=1$ is presented by blue lines marked with down triangles, $\alpha=3$ is shown by green lines marked with squares, and $\alpha=10$ is presented by red lines and up triangles.

is calculated as $\gamma_{av}=0.5(\gamma_{\max}+\gamma_{\min})$. Again, one can conclude that the relative energy spread for the REM electrons can be very small for small values of $\alpha$. Thus, for $\alpha=1$, its value is about 2.5% for all considered values of $a_0$ that can be enough for many applications.

It is interesting to note that such a small energy spread is characteristic not only near time $t_{\gamma\max}$ but it is also typical for all evolution of the REM until time $t_{\gamma\max}$. To demonstrate this feature, the values for $p_z$, $p_y$, and $\gamma$ as functions of time are presented in Fig. 10 for the case of $\alpha=1$ and $a_0=6$. These data were calculated with the code EXACT. Figure 10 proves that one can effectively use the REM until time $t_{\gamma\max}$.

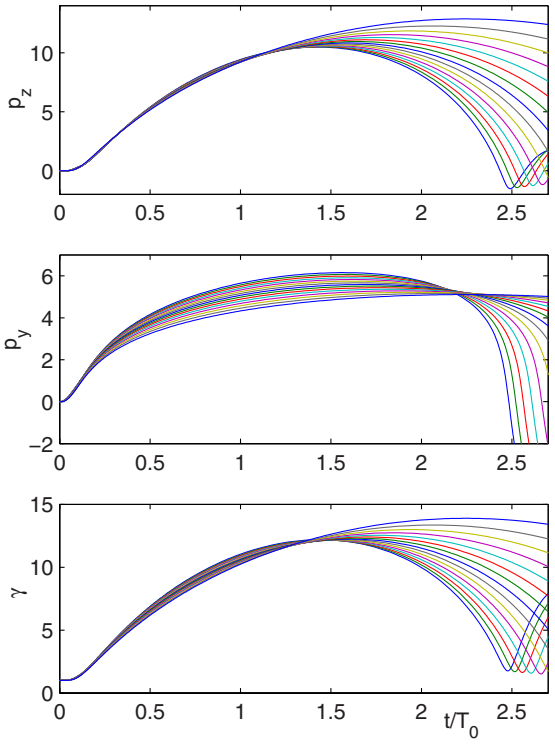


FIG. 10. (Color online) Longitudinal momenta, transverse momenta, and energy of some ESs of the REM as functions of time for $a_0=6$ and $\alpha=1$.

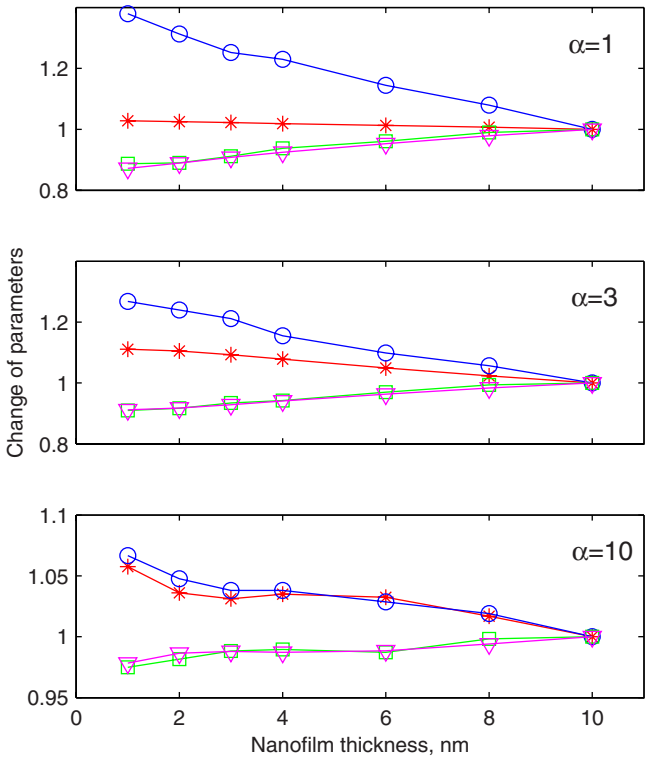


FIG. 11. (Color online) Dependence of the REM parameters [the energy (red stars), the thickness $l_\gamma$ at time $t_{\gamma\max}$ (blue circles), the lifetime $t_l$ of the REM (magenta triangles), and the time $t_{\gamma\max}$, when the energy of the left REM electrons reaches maximum (green squares)] on nanofilm thickness for $\alpha$ equals 1, 3, and 10 and $a_0=6\alpha$. All parameters are normalized with their values at $l=10$ nm. Note different vertical scale for the first two plots and the last one.

## V. DEPENDENCE OF THE REM PARAMETERS ON NANOFILM THICKNESS

In the simulations of Sec. IV, we suppose that the nanofilm thickness is constant, while the density and, correspondingly, $\alpha$ were changed. In principle, this situation can be realized in experiment using solid-state density nanofilms with variable thickness. To prepare the state of the target, two additional counterstreaming heating laser prepulses are necessary in this case. Then, some time after the heating of prepulses, the density of the target will be decreased with corresponding increase in the thickness. However, the experimental scheme becomes rather complicated in this case, besides, the precise timing is necessary. Let us now investigate how the change in the initial thickness influences the REM parameters. We will use the 1D code EXACT [50] to calculate the parameters of the REM since the 2D PIC simulations turned out to be rather time demanding for required accuracy of simulations when the thickness of the target is around 1 nm.

In Fig. 11, the changes in the REM parameters (normalized with their values for the thickness of 10 nm) are shown for $\alpha$ equal to 1, 3, and 10 and $a_0=6\alpha$. In these simulations,

the initial density of the nanofilm was changed in accordance with the initial thickness of the target such that $\alpha \sim n_0 l$ was kept fixed, i.e., the initial densities for the most left points are ten times larger than for the most right points on these plots. One can make several conclusions based on these figures. First of all, the thickness of the REM, $l_\gamma$, at time $t_{\gamma\,\max}$ increases with decrease in the initial thickness of the REM (the same effect was observed in [45]) with correspondent increase in the maximal energy, while the lifetime decreases, i.e., the better REM parameters can be achieved for the larger initial thickness of the nanofilm and less initial density (for fixed $\alpha$). Then, one can conclude that the REM parameters really depend on the nanofilm thickness relatively weakly: the change in the nanofilm thickness by ten times causes less than 40% change in the thickness $l_\gamma$ and less than 20% change in the other REM parameters. Moreover, for large $\alpha$ values, i.e., $\alpha \sim 10$, the change in all REM parameters is less than 7% that confirms our assumptions for deriving the approximate analytical solutions. Also, the curves for $t_{\gamma\,\max}$ practically coincide with the curves for $t_l$ so the dynamical evolution of the REM scales according to $t_l$. And at last, the change in the maximal energy of the REM electrons is negligible for small $\alpha$, while it practically follows the thickness curve for $\alpha = 10$.

## VI. SCALING OF THE REM PARAMETERS WITH $\alpha$ AND $a_0$

In Sec. III, the approximate analytical solutions were presented for the generation of the REM. In Sec. IV, these analytical solutions were compared with the 2D PIC simulations and a good correspondence was ascertained. In this section, the scaling with $\alpha$ and $a_0$ of the maximal values for the REM dynamical parameters will be analyzed based on the analytical solutions.

Generally speaking, all dynamical variables $p_y$, $p_z$, and $\gamma$ achieve their maxima at different values of parameters $\theta_0$ and $\theta_l$. To get the order of value estimates, we will consider the maximum for $|p_y|$ only supposing that the maxima of other variables are situated not far from the maximum for $|p_y|$. We will also omit the exponential terms in Eqs. (10) because their influence is small far from the initial point $\theta_0 = \theta_l = 0$. Then, the absolute value for the transverse momentum $p_{yl}$ of the right electrons achieves its maximum,

$$|p_{yl\,\max}| = \frac{a_0}{\sqrt{1+\alpha^2}}, \tag{12}$$

at

$$\theta_{l\,\max} = \frac{\pi}{2} + \arctan \alpha^{-1}. \tag{13}$$

For estimating the maximum of $|p_{y0}|$ for the left electrons, we will again suppose that $\kappa_0$ is a slow variable (cf. derivation of the solution for $p_{y0}$). Then, one gets

$$|p_{y0\,\max}| = \frac{a_0 \kappa_0}{\sqrt{\kappa_0^2 + \alpha^2}},$$

$$\theta_{0\,\max} = \frac{\pi}{2} + \arctan \frac{\kappa_0}{\alpha}. \tag{14}$$

It is possible to distinguish two different cases for combination of the REM parameters. In the first case, the parameter $\alpha$ is not very large and $\alpha^2 \theta_{0\,\max}/a_0 \ll 1$. Then, $\kappa_0 \simeq 1$, i.e., the role of Coulomb and radiation reaction forces is not very important. In this case, the estimates for $|p_{y0\,\max}|$ and $\theta_{0\,\max}$ are defined by the same expressions [Eqs. (12) and (13)], which were derived for $|p_{yl\,\max}|$ and $\theta_{l\,\max}$ above. So $\theta_{0\,\max} < \pi$ and the condition for this first case has the form $\pi\alpha^2/a_0 \ll 1$. The maxima for the longitudinal momentum and the energy are approximately the same for the left and for the right electrons and can be obtained from Eqs. (6) as follows:

$$\gamma_{\max} = 1 + \frac{a_0^2}{2(1+\alpha^2)},$$

$$p_{z\,\max} = \frac{a_0^2}{2(1+\alpha^2)}. \tag{15}$$

This case constitutes the regime of the small energy spread considered numerically in Sec. V.

For the second case, the parameter $\alpha$ is large and $\alpha^2 \theta_{0\,\max}/a_0 \gg 1$. Then $\kappa_0$ can be estimated as $\kappa_0 \simeq \alpha^2 \theta_{0\,\max}/a_0$; however, still $\kappa_0/\alpha \simeq \alpha \theta_{0\,\max}/a_0 < 1$ since, for generation of the REM, one need to achieve the certain threshold in the laser amplitude in accordance with Eq. (11). So in this case, one has limitation $\theta_{0\,\max} < 3\pi/4$, and the condition for validity of this case reads $3\pi\alpha^2/(4a_0) \gg 1$. For the maxima of dynamical parameters one has

$$|p_{y0\,\max}| \simeq \alpha \theta_{0\,\max},$$

$$\gamma_{0\,\max} \simeq p_{z0\,\max} \simeq \frac{a_0 \theta_{0\,\max}}{2}. \tag{16}$$

For estimates, one can use in these expressions the value from $\pi/2$ to $3\pi/4$ for $\theta_{0\,\max}$ depending on the value of $\alpha/a_0$. Here, the linear scaling of the maximal energy with $a_0$ is due to the strong collective radiation friction force [24,50] (cf. also Sec. IV).

Scalings (12), (15), and (16) were compared with the corresponding values obtained from the 2D PIC simulations of Sec. IV. This comparison shows that estimates (12), (15), and (16) are valid within a factor of 2 for all range of considered parameters.

Let us now estimate the lifetime $t_l$ of the REM, i.e., the time when $p_{z0} = 0$. From Eqs. (10), using equation $\omega t \simeq k Z_0$ to estimate $t_l$ and omitting $\kappa_0$ with respect to $\alpha$, one gets

$$\omega t_l \simeq \frac{a_0^2}{4\alpha^2}\left[\theta_{0\mathrm{end}} - \frac{\sin 2\theta_{0\mathrm{end}}}{2}\right], \tag{17}$$

where $p_{z0} = 0$ for $\theta_{0\mathrm{end}}$. For the order of value estimates, one can use $\pi$ for $\theta_{0\mathrm{end}}$, and finally, the lifetime is estimated as

$$t_l \simeq \frac{a_0^2}{8\alpha^2} T_0. \tag{18}$$

This estimate coincides with the results of the 2D PIC simulations of Sec. IV within a factor of 2, giving the relative error of less than 20% for the case of $\alpha=10$.

## VII. DISCUSSION OF RESULTS AND CONCLUSION

Now, let us consider some examples. According to our theory and simulations, the initial diameter of the REM is equal to the laser beam diameter $2w_0$, and the initial charge is proportional to $w_0^2\alpha$. The laser power for $w_0 \approx 8\lambda$ and $a_0=60$ amounts to 5 PW and the charge of the REM (estimated inside $2w_0$ spot) is 160 nC ($10^{12}$ electrons) for $\alpha=10$. For $w_0 \approx 2\lambda$, the values are more modest: 300 TW and 10 nC ($6.25\times10^{10}$ electrons), and this power can be already realized nowadays. For the proof-of-principle experiments, using, e.g., graphene sheets [32–34] as a target ($l=2$ nm, $\alpha \simeq 2$) and with a laser spot size of about $w_0 \simeq \lambda$, the laser power of 2 TW is enough.

The parameters of the REM are very sensitive to the value of $\alpha$, i.e., to the initial thickness of the nanofilm. Small values of $\alpha \sim 1$ allow us to achieve quasimonochromatic regime of the REM generation with the relative energy spread of less than several percents. Also, for a fixed value of the laser pulse amplitude $a_0$, the energy of the REM electrons is higher for smaller $\alpha$. However, the charge of the REM is directly proportional to $\alpha$, so, for application of the REM as a reflector for a scattering of a counterstreaming probe laser pulse, some trade-off is possible. In other applications, the REM parameters can be adjusted for required values.

If the laser pulse has a smooth front, then the electrons of the REM remain motionless in the longitudinal direction until the laser amplitude reaches the value $a_0 \sim \alpha$ [24,48]. After that, the electrons will be displaced longitudinally by the first half-cycle, which has the amplitude $a_{0f}$ larger than $\alpha$. To really form the REM, for which $t_l > T_0$, the amplitude $a_{0f}$ should be greater than $a_{0th}$. Then, the REM will evolve until the turn of the left electrons and the lifetime will be greater for larger values of $a_{0f}/\alpha$. This picture is confirmed by our 2D PIC simulations. So for the generation of a good REM by a smooth laser pulse, the high peak-to-peak ratios of $\sim 4-5$ are necessary at the front of the laser pulse [for a Gaussian longitudinal profile, it corresponds to a full duration at half maximum of about $(1.2 \sim 1.4)\lambda$]. More detailed study of this issue will be presented in the forthcoming publication.

For a real three-dimensional case, one can expect an increase in the lifetime of the REM due to decrease in Coulomb attraction from the ions' background. However, this effect can be evident only for a very high intensity of the laser beam when the quasi-one-dimensional approximation fails. In this case, the longitudinal displacement of the REM should be much larger than its diameter. The other effect for the REM with a large lifetime (large $a_0$) can be the compensation of the ions' background by the nanofilm electrons. These two effects can improve the parameters of the generated REM, however, rather high laser intensities are necessary. Long-term evolution of the REM after turning back of the left electrons will be considered in the forthcoming paper.

In conclusion, we proposed and investigated the application of a nanofilm for the generation of a single attosecond high-charge relativistic electron bunch with predefined parameters. With the 2D PIC simulations, we studied the REM characteristics in a regular way for a wide range of parameters. For different parameters $\alpha$ of the nanofilm, we determined the laser amplitude threshold for the process of the REM generation. Also, we found by simulations the dependences of the maximal energy of electrons, the energy spread, and the lifetime of REM on the field amplitude and $\alpha$. We verified the developed 1D self-consistent theory with the 2D PIC simulation results and found a good agreement. The theory takes into account Coulomb interactions, radiation of the electrons, and laser amplitude depletion. Using 1D simulations, we investigated the dependence of the REM parameters on nanofilm thickness (while $\alpha$ was kept fixed) and found rather week dependence. And finally, the scaling of the REM dynamical parameters with the field amplitude and the nanofilm thickness is analyzed. This scaling shows that the energy and the energy spread of the electrons in the REM are controlled by $a_0$ and $\alpha$. For small value of $\alpha$, the quasimonochromatic regime of the REM generation can be achieved.

## ACKNOWLEDGMENTS

This work was supported by the Ministry of Knowledge and Economy of Korea through the Ultrashort Quantum Beam Facility Program, by the GIST Top Brand Project "Photonics 2020,"and by RFBR Project No. 09-02-01483-a. We thank Professor W. Mori at UCLA for the OSIRIS code.

[1] Y. Tabata, Radiat. Phys. Chem. **18**, 43 (1981).
[2] *Ultrafast Phenomena*, edited by P. F. Barbara, W. H. Knox, G. A. Mourou, and A. H. Zewail (Springer-Verlag, Berlin, 1994), Vol. IX, and references cited therein.
[3] R. A. Crowell, D. J. Gosztola, I. A. Shkrob, D. A. Oulianov, C. D. Jonah, and T. Rajh, Radiat. Phys. Chem. **70**, 501 (2004).
[4] D. Umstadter, J. K. Kim, and E. Dodd, Phys. Rev. Lett. **76**, 2073 (1996).
[5] A. J. W. Reitsma, V. V. Goloviznin, L. P. J. Kamp, and T. J. Schep, Phys. Rev. E **63**, 046502 (2001).
[6] E. Esarey, S. K. Ride, and P. Sprangle, Phys. Rev. E **48**, 3003 (1993).
[7] B. K. Agarwal, *X-Ray Spectroscopy: An Introduction*, 2nd ed. (Springer, Berlin, 1991).
[8] *Applications of X-Rays Generated from Lasers and Other Bright Sources*, edited by G. A. Kyrala and J.-C. Gauthier, Proc. SPIE Vol. 4504 (2001).
[9] A. Rousse, C. Rischel, and J. C. Gauthier, Rev. Mod. Phys. **73**,

17 (2001).
[10] S. B. Dierker, R. Pindak, R. M. Fleming, I. K. Robinson, and L. Berman, Phys. Rev. Lett. **75**, 449 (1995).
[11] P. Cloetens, W. Ludwig, J. Baruchel, D. Van Dyck, J. Van Landuy, J. P. Guigay, and M. Schlenker, Appl. Phys. Lett. **75**, 2912 (1999).
[12] G. J. Williams, M. A. Pfeifer, I. A. Vartanyants, and I. K. Robinson, Phys. Rev. Lett. **90**, 175501 (2003).
[13] R. Kodama, K. A. Tanaka, Y. Sentoku, T. Matsushita, K. Takahashi, H. Fujita, Y. Kitagawa, Y. Kato, T. Yamanaka, and K. Mima, Phys. Rev. Lett. **84**, 674 (2000).
[14] N. Naumova, I. Sokolov, J. Nees, A. Maksimchuk, V. Yanovsky, and G. Mourou, Phys. Rev. Lett. **93**, 195003 (2004).
[15] S. D. Baton *et al.*, Phys. Rev. Lett. **91**, 105001 (2003).
[16] J. Zheng, K. A. Tanaka, T. Sato, T. Yabuuchi, T. Kurahashi, Y. Kitagawa, R. Kodama, T. Norimatsu, and T. Yamanaka, Phys. Rev. Lett. **92**, 165001 (2004).
[17] A. G. Khachatryan, F. A. van Goor, and K.-J. Boller, Phys. Rev. ST Accel. Beams **7**, 121301 (2004).
[18] N. Hafz *et al.*, Appl. Phys. Lett. **90**, 151501 (2007).
[19] G. V. Stupakov and M. S. Zolotorev, Phys. Rev. Lett. **86**, 5274 (2001).
[20] V. V. Kulagin *et al.*, Phys. Lett. A **353**, 505 (2006).
[21] V. V. Kulagin, V. A. Cherepenin, M. S. Hur, J. Lee, and H. Suk, Laser Part. Beams **26**, 397 (2008).
[22] V. A. Cherepenin and V. V. Kulagin, Phys. Lett. A **321**, 103 (2004).
[23] V. V. Kulagin, V. A. Cherepenin, and H. Suk, Appl. Phys. Lett. **85**, 3322 (2004).
[24] V. V. Kulagin, V. A. Cherepenin, and H. Suk, Phys. Plasmas **11**, 5239 (2004).
[25] V. V. Kulagin, V. A. Cherepenin, M. S. Hur, and H. Suk, Phys. Rev. Lett. **99**, 124801 (2007).
[26] M. Y. Shverdin, D. R. Walker, D. D. Yavuz, G. Y. Yin, and S. E. Harris, Phys. Rev. Lett. **94**, 033904 (2005).
[27] A. Guandalini *et al.*, J. Phys. B **39**, S257 (2006).
[28] G. A. Mourou, T. Tajima, and S. V. Bulanov, Rev. Mod. Phys. **78**, 309 (2006).
[29] A. Valenzuela and J. C. Eckardt, Rev. Sci. Instrum. **42**, 127 (1971).
[30] R. V. Volkov *et al.*, Kvantovaya Elektron. (Moscow) **24**, 1114 (1997) [Quantum Electron. **27**, 1081 (1997)].
[31] D. J. McComas, F. Allegrini, C. J. Pollock, H. O. Funsten, S. Ritzau, and G. Gloeckler, Rev. Sci. Instrum. **75**, 4863 (2004).
[32] K. S. Novoselov *et al.*, Science **306**, 666 (2004).
[33] K. S. Novoselov *et al.*, Proc. Natl. Acad. Sci. U.S.A. **102**, 10451 (2005).
[34] A. K. Geim and K. S. Novoselov, Nature Mater. **6**, 183 (2007).
[35] T. Stoebe, P. Mach, and C. C. Huang, Phys. Rev. Lett. **73**, 1384 (1994).
[36] M. Conradi, M. Cepic, M. Copic, and I. Musevic, Phys. Rev. Lett. **93**, 227802 (2004).
[37] M. Veum, E. Kutschera, N. Voshell, S. T. Wang, S. L. Wang, H. T. Nguyen, and C. C. Huang, Phys. Rev. E **71**, 020701(R) (2005).
[38] W. Yu, V. Bychenkov, Y. Sentoku, M. Y. Yu, Z. M. Sheng, and K. Mima, Phys. Rev. Lett. **85**, 570 (2000).
[39] K. Miyauchi, S. Miyazaki, K. Sakai, S. Kawata, Q. Kong, A. A. Andreev, and T. Kikuchi, Phys. Plasmas **11**, 4878 (2004).
[40] T. Plettner, R. L. Byer, E. Colby, B. Cowan, C. M. S. Sears, J. E. Spencer, and R. H. Siemann, Phys. Rev. Lett. **95**, 134801 (2005).
[41] J. Meyer-ter-Vehn and H.-C. Wu, http://arxiv.org/abs/0812.0710.
[42] T. Baeva, S. Gordienko, and A. Pukhov, Laser Part. Beams **25**, 339 (2007).
[43] E. L. Saldin, E. A. Schneidmiller, and M. V. Yurkov, Opt. Commun. **281**, 1179 (2008).
[44] H.-C. Wu and J. Meyer-ter-Vehn, http://arxiv.org/abs/0812.0703.
[45] M. Wen, H.-C. Wu, J. Meyer-ter-Vehn, and B. Shen, http://arxiv.org/abs/0812.0700.
[46] R. G. Hemker, Ph.D. thesis, UCLA, 2000.
[47] J. P. Verboncoeur, A. B. Langdon, and N. T. Gladd, Comput. Phys. Commun. **87**, 199 (1995).
[48] V. A. Vshivkov *et al.*, Phys. Plasmas **5**, 2727 (1998).
[49] B. Rau, T. Tajima, and H. Hojo, Phys. Rev. Lett. **78**, 3310 (1997).
[50] V. V. Kulagin, V. A. Cherepenin, M. S. Hur, and H. Suk, Phys. Plasmas **14**, 113101 (2007).
[51] L. D. Landau and E. M. Lifshitz, *The Classical Theory of Fields* (Nauka, Moscow, 1988); *The Classical Theory of Fields* (Pergamon, Oxford, 1975), Chap. 6, Sec. 48.